Neural Network Based Irradiance Mapping Model of Solar PV Power Forecasting Using Sky Image

Fei Wang
State Key Laboratory of Alternate Electrical Power System with Renewable Energy Sources (North China Electric Power University), Baoding 071003, China; also with Department of Electrical Engineering, North China Electric Power University, Baoding 071003, China; also with Hebei Key Laboratory of Distributed Energy Storage and Micro-grid (North China Electric Power University) Baoding 071003, China
feiwang@ncepu.edu.cn

Dashuai Ma
State Grid Suzhou Power Supply Company
Suzhou 234000, China
gszgdmds@sina.com

Miadreza Shafie-khah
C-MAST, University of Beira Interior
6201-001 Covilhã, Portugal
miadreza@ubi.pt

Xinxin Ge, Zhao Zhen, Hui Ren and Yajing Gao
Department of Electrical Engineering
North China Electric Power University
Baoding 071003, China
zhenzhao@ncepu.edu.cn

João P. S. Catalão
INESC TEC and FEUP, 4200-465 Porto, Portugal;
also with C-MAST/UBI, 6201-001 Covilhã, Portugal;
also with INESC-ID, IST-UL
1049-001 Lisbon, Portugal
catalao@ubi.pt

***Abstract*—Due to the stochastic fluctuant characteristic of solar irradiance, large-scale grid-connected photovoltaic (PV) power plants can bring great difficulties to the operation of the power system. In order to fulfil the sky images based ultra-short term PV power forecasting and enhance the grid consumptive ability of PV power, an accurate model that can map sky images to corresponding surface solar irradiance is very significant. Therefore, in this paper a neural network based irradiance mapping model of solar PV power forecasting using sky image is proposed. First, we combine the theoretical calculation of extraterrestrial solar irradiance and atmospheric optical thickness to establish the clearance surface irradiance model. Second, the sky images observed by total sky imager are processed to extract image features related to solar irradiance. Third, a neural network based irradiance mapping model is built and trained using historical sky images and solar irradiance data. Simulation results show that the proposed model can map sky image features to surface solar irradiance accurately in different weather conditions.**

***Index Terms*—PV power forecasting, irradiance mapping model, sky image, neural network**

I. INTRODUCTION

With the energy crisis and environmental pollution problems become increasingly serious, the demand for renewable energy such as solar power is increasing [1]–[3]. Solar irradiance is the main factor that affects the solar PV power output[4].

Due to the stochastic fluctuant characteristic of solar irradiance, large-scale grid-connected photovoltaic (PV) power plant can bring great difficulties to the operation of power system [5]–[7].

PV power forecasting is an effective way to solve the above problems [8]–[12]. While in cloudy weather, the forecast accuracy of PV power declined significantly due to the fluctuation of irradiance caused by clouds movement [13]. Focus on the irradiance fluctuation under the effect of clouds, some ultra-hour irradiance forecasting methods based on cloud image analysis have been developed in recent years [14]–[17]. For these ultra-short term or minute time scale PV power forecasting approaches, sky images are key data resources. Accurate calculation of solar irradiance using sky images can effectively improve the performance and accuracy of sky image based PV power forecasting model [18]–[20].

However, most of the above researches pay little attention to the mapping model from sky images to surface solar irradiance value. Usually, the forecast of future sky images cannot be very precise due to the growth and deformations of cloud. In this condition, if we use the forecasted sky images as model inputs directly to map the surface solar irradiance, the results could be inaccurate as well. Therefore, it is very necessary to extract features of sky images that can effectively reflect the situation of surface irradiance meanwhile is robust to the deformation of cloud.

In this paper we proposed a neural network based irradiance mapping model of solar PV power forecasting using sky image to realize the surface irradiance calculation.

First, we combine the theoretical calculation of extraterrestrial solar irradiance and atmospheric optical thickness to establish the clearance surface irradiance model. Second, the sky images observed by total sky imager are processed to extract image features related to solar irradiance.

Third, a neural network based irradiance mapping model is built and trained using historical sky images and solar irradiance data. The National Renewable Energy Laboratory collects the data used in this paper for model training and simulation test.

II. MODEL FRAMEWORK

According to the fundamentals of atmospheric radiative transfer algorithm, when in sunny clear sky weather conditions, the solar radiation will not only be absorbed by vapor and ozone, but also scattered by air molecules and aerosols. These influence factors of solar irradiance are depending on the local atmospheric environment and are relatively stable.

However, in cloudy weather conditions, besides the above factors, the solar irradiance will also be absorbed and reflected by cloud as well. Due to the movement of cloud and changing relative position between cloud and sun, the solar irradiance that can reach the surface is highly fluctuated. Therefore, the local atmospheric environment and cloud distribution can be considered as the main influence factors of surface solar irradiance.

Based on the above analysis, a framework of irradiance mapping model using sky image is proposed as shown in Fig 1. First, we combine the theoretical calculation of extraterrestrial solar irradiance and atmospheric optical thickness to establish the clearance surface irradiance model. Second, the sky images observed by total sky imager are processed to extract image features related to solar irradiance. Third, a neural network based irradiance mapping model is built and trained using historical sky images and solar irradiance data.

III. MODEL INPUT

A. Clear sky surface solar irradiance

The surface solar irradiance changes over time and is influenced by various constituents in the atmosphere. Because of the revolution and rotation of the earth, the extraterrestrial irradiance is changes periodically and can be calculated according to a series of astronomical parameters, including declination angle, earth-sun distance, solar hour angle, and solar elevation, as shown in the following functions [21]:

$$\delta = 23.45 * \sin(360 \times \frac{n+284}{365}) \tag{1}$$

$$r = 1 + 0.034 \times \cos(\frac{2\pi n}{365}) \tag{2}$$

$$\omega = (t - 12) \times 15 \tag{3}$$

$$h = \arcsin(\sin\varphi \sin\delta + \cos\varphi \times \cos\delta \times \cos\omega) \tag{4}$$

where δ is solar declination angle, n is ahargana, ω is solar hour angle, t is true solar time, φ is latitude, and h is solar elevation.

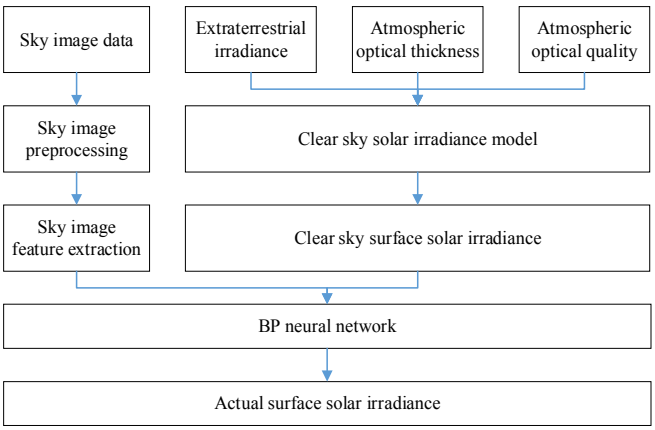

Fig. 1. Neural network based irradiance mapping model framework

Under clear sky conditions, when solar radiation passing through the atmosphere, some part is reflected to the outer space, some part is absorbed and scattered by vapor, air molecules, and aerosols. The direct normal irradiance E_b and diffuse irradiance E_d that reach the surface are calculated as:

$$E_b = E_{SC} \times r \times e^{-\tau^b m^b} \tag{5}$$

$$E_d = E_{SC} \times e^{-\tau^d m^d} \tag{6}$$

where E_{sc} is solar constant which equals to 1366.1W/m^2, τ_b and τ_d is the optical thickness of direct irradiance and diffuse irradiance. The values of τ_b and τ_d depend on local environment and their reference values are provided by [22]. b and d are the modification indexes of atmospheric optical quality of direct irradiance and diffuse irradiance, and can be calculated using τ_b and τ_d. m is atmospheric optical quality and can be calculated using h. Therefore, the clear sky surface irradiance can be calculated as:

$$E_h = E_b + \sinh + E_d \tag{7}$$

B. Sky image feature extraction

Compared with vapor, air molecules, and aerosols, the influence of cloud on surface irradiance is greater and with higher randomness. Sky image can provide detail information of cloud to help calculate the actual surface irradiance.

TSI-800 is an automatic full color imaging system, which can capture and real-time process the sky images. The TSI is consist of a hemispherical mirror and a CCD camera. On the hemispherical mirror, there is a shading plate move follow the sun to protect the camera from direct sunlight.

The TSI and its output sky image are shown in Fig 2. To better recognize the cloud in sky image, the noises such as the view of support arm, shading plate, and other irrelevant pixels need to be filtered. As the position support arm is fixed, and the position of shading plate is determined by solar azimuth, we can obtain the processed image as shown in Fig 3.

(a)

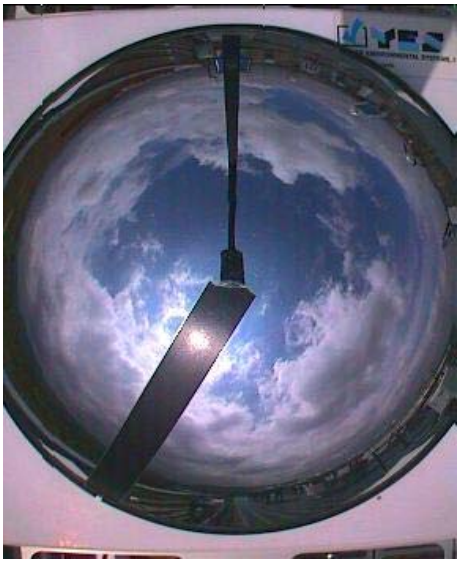

(b)

Fig. 2. TSI-800 and its output image

Fig. 3. The processed image

Cloud is the most important influence factors of surface irradiance. Therefore, the accurate recognition of cloud pixels is the prerequisite of surface irradiance calculation.

For different cloud types, their influence level on surface irradiance is different as well. Generally, the lower and thicker of the cloud, the stronger ability to reduce solar radiation; the higher and thinner of the cloud, the weaker ability to reduce the solar radiation. In this paper, all the cloud are classified into two classes of strong shading clouds and weak shading clouds. In a sky image, the solar region is centered on the sun and with a radius of 50 pixels.

After the installation of TSI is completed, the position of sun has a fixed function relationship with the solar altitude angle, which can be fitted using historical data. In the solar region, the weak shading clouds show a white color due to the sunshine, while strong shading clouds and sky usually show dark color.

Therefore, the brightness L can be used to recognize the weak shading clouds, which can be calculated using the value of R, G, and B channels:

$$L = (R + G + B)/3 \tag{8}$$

To recognize strong shading clouds, we use the tradition red blue ratio method, the normalized red blue ratio NBR is:

$$NBR = \frac{B - R}{B + R} \tag{9}$$

Suppose the threshold of L is T_1, the threshold of NBR is T_2, the belongings of image pixels can be determined according to function (10).

$$C = \begin{cases} \text{weak shading clouds} & L > T_1 \\ \text{strong shading clouds} & L < T_1, NBR \le T_2 \\ \text{clear sky} & L < T_1, NBR > T_2 \end{cases} \tag{10}$$

As shown in Fig 4, the solar region is circled with red line.

Fig 5 is the cloud recognition results, in which the blue pixels represent clear sky, white pixels represent weak shading clouds, and re pixels represent strong shading clouds.

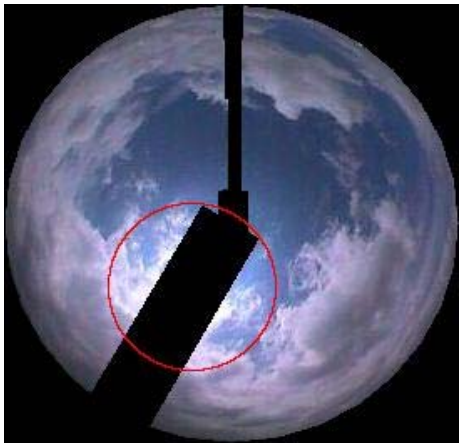

Fig. 4. Solar region

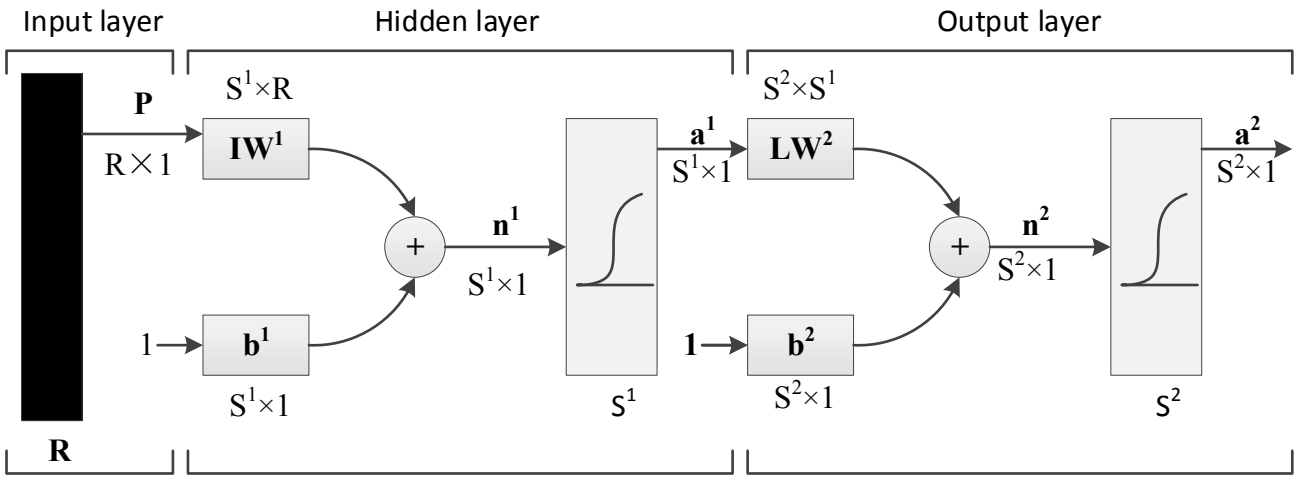

Fig. 5. BP neural network model

Suppose the number of pixels of weak shading clouds, strong shading clouds, and clear sky are N_c, N_{vc}, and N_s respectively, the cloud cover ratio of weak shading clouds M_c and strong shading clouds M_{vc} can be calculated by the following functions.

$$M_c = N_C /(N_C + N_{VC} + N_S) \tag{11}$$

$$M_{VC} = N_{VC} /(N_C + N_{VC} + N_S) \tag{12}$$

IV. MODEL DESIGN

A. BP neural network

The neural network has strong nonlinear fitting ability. Theoretically, a neural network is capable of approximating any nonlinear continuous function with arbitrary precision, which make it be widely used in solar forecasting researches. In this paper, a common BP neural network is applied to build the proposed irradiance mapping model [23], [24].

BP neural network is a multilayer feedforward neural network consist of input layer, hidden layer, and output layer. In training process the neural network can learn the mapping relation between input and output, and record the learning results as network weights. Fig 6 shows a typical two-layer BP neural network model.

In this neural network model, P is input vector, IW^1 is the weight vector between input layer and hidden layer, b^1 is the threshold vector of hidden layer, S^1 is the excitation function of hidden layer, LW^2 is the weight vector between hidden layer and output layer, b^2 is the threshold vector of output layer, S^2 is the excitation function of output layer, a^2 is the output vector. According to Figure 6, there will be:

$$a^1 = S^1\left(P \cdot IW^1 + b^1\right) \tag{13}$$

$$a^2 = S^2\left(a^1 \cdot LW^2 + b^2\right) \tag{14}$$

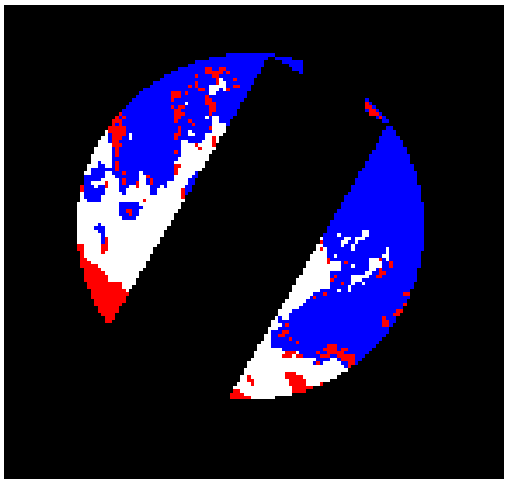

Fig. 6. Cloud recognition results

The BP neural network has many characteristics of the human brain. When the external environment changes, the network will change the weight vector as well according to the input signals, so as to adopt to the mapping relationship from input signals to output data. This training and learning process of BP neural network can be divided into two stages:

1) Enter the known learning samples, set the network structure, weight and threshold. The output of each neuron is calculated backwards from the first layer of the network.

2) Calculate the influence of weight and threshold on network error, and then modify the weight and threshold according to the errors.

B. Network training

The input vector and the network topology together determine the performance of the model. To achieve better irradiance mapping results, the input vector should contain comprehensive information about solar radiation.

According to the principles of atmospheric radiation transfer, the extraterrestrial irradiance will be absorbed and scattered by vapor, aerosols, ozone, and clouds before reach the ground.

During the transfer process, the influence of vapor, aerosols, and ozone is relatively small, and usually unchanged in the day. While the influence of cloud is obvious and changes rapidly. Therefore, we choose the clear sky surface solar irradiance $E_h(t)$, weak shading clouds cover ratio $M_c(t)$, and strong shading clouds cover ratio $M_{vc}(t)$ at time point t as model input, and choose the actual surface solar irradiance $I(t)$ as model output to train the BP neural network.

The node number of input layer, hidden layer, and output layer, determines the network topology. For input and output layers, the node number corresponds to the number of input and output factors. The node number of hidden layer has a great influence on the performance of the network, but its selection is also very complex.

In this paper, based on the empirical formula (15) and tests, the node number of hidden layer is set to 7 [25]–[27].

$$n = \sqrt{n_i + n_o} + a \tag{15}$$

where n is node number of hidden layer, n_i is node number of input layer, n_o is node number of output layer, a is constant value between 1 to 10.

The excitation function of BP neural network usually use the sigmoid function, its output is limited to a small scale as 0 to 1 or -1 to 1. In this paper, the excitation functions of hidden layer and output layer are all hyperbolic tangent sigmoid excitation function.

V. SIMULATION

The National Renewable Energy Laboratory collects the data used in this paper for model training. Mean absolute error (MAE) and root mean square error (RMSE) are applied to evaluate the performance and accuracy of the proposed irradiance mapping model [28]. The MAE and RMSE can be calculated by formula (16) and (17).

$$MAE = \frac{1}{n}\sum_{i}^{n}\left|\hat{Y}_i - Y_i\right| \tag{16}$$

$$RMSE = \sqrt{\frac{1}{n}\sum_{i}^{n}\left(\hat{Y}_i - Y_i\right)^2} \tag{17}$$

where $\hat{Y}_i$ is calculation value, Y_i is actual value, n is sample number. The solar irradiance data and sky image data from May 26, 2016 to May 30 is used to test the mapping model. The calculated surface irradiance using mapping model and actual surface irradiance are shown in Fig 7.

The calculation error of the irradiance mapping model is shown in Table I.

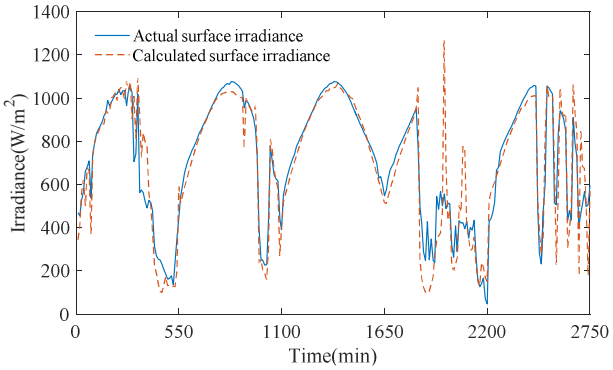

Fig. 7. Actual and calculated surface irradiance

TABLE I
CALCULATION ERROR

date	MAE(W/m^2)	RMSE(W/m^2)
26	79.52	117.52
27	58.38	40.44
28	23.83	27.96
29	110.62	164.67
30	83.77	119.21
26~30	67.64	108.93

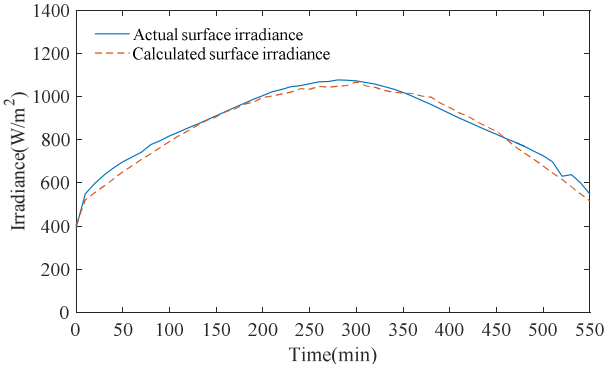

Fig. 8. Calculation results on May 28th

May 30th is cloudy day, the cloud covered the sun several times during the day, which resulting in fluctuations in irradiance. The calculation results are shown in Fig 9. It can be seen that the mapping model can recognize the irradiance fluctuation very well.

Fig 10 shows the calculation results on May 29th. The weather type is cloudy. It can be seen that the calculation results only close to the actual value in trend. The calculation error is relatively large compared with other days' results. Especially at the time point t, the absolute error of calculation result reaches the maximum.

To find out the causes of this kind of high error, we find out the sky image and corresponding cloud recognition results at the time point *t*, as shown in Fig 11 and Fig 12.

It can be seen that the sky environment around the sun is very complex and the tone of the picture is darker. In this condition, many sky pixels are recognized as thick cloud pixels, which cause the cloud recognition result is not very accurate and influence the surface irradiance calculation.

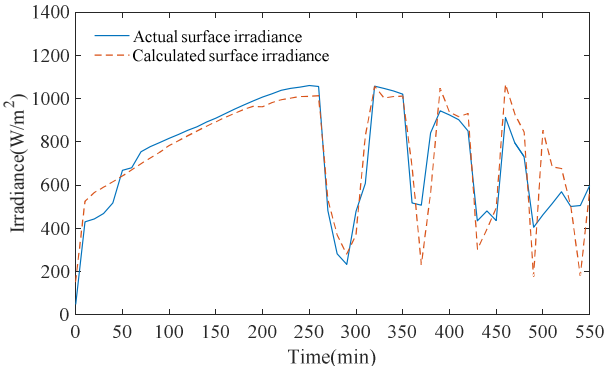

Fig. 9. Calculation results on May 30th

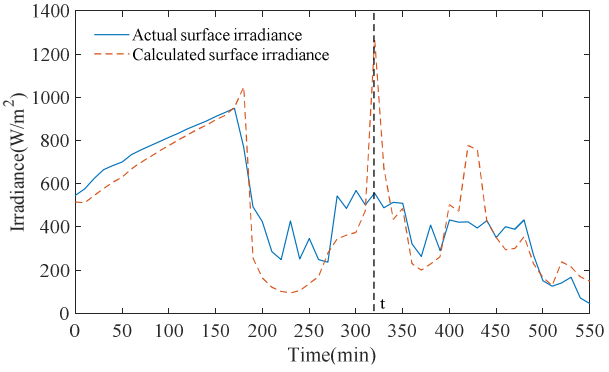

Fig. 10. Calculation results on May 29th

Fig. 11. Sky image

Fig. 12. Cloud recognition results

VI. CONCLUSION

Accurate calculation of surface irradiance requires a comprehensive consideration of solar irradiance influence factors. In this paper, we analyzed the astronomical factors that affect the cyclical changes of surface solar irradiance and the meteorological factors that affect the random changes. Then, a surface irradiance mapping model realized by neural network is proposed to calculate surface irradiance using sky image data. The input variables of the irradiance mapping neural network model are studied as well. First, we analyze the influence of cloud, water vapor, aerosol, and atmospheric molecules on the attenuation of solar irradiance during the process of solar radiation passing through the atmosphere. Then, we combine the theoretical calculation of extraterrestrial solar irradiance and atmospheric optical thickness to establish the clearance surface irradiance model. Second, the sky images observed by total sky imager are preprocessed before application, including the marking and filtering of interfering objects in sky images, image distortion correction, cloud identification. In the end, we introduce the clearance surface irradiance, thick cloud cover, thin cloud cover, temperature, wind speed and other related influence factors as the input variables of irradiance mapping neural network to calculate the surface irradiance. Then, an optimal input variable combination is determined by comparing the results of different combinations of input variables. Model structure and parameters are also optimized based on historical data. Simulation results show that the proposed irradiance mapping model can achieve the calculation of surface solar irradiance accurately.

ACKNOWLEDGEMENT

This work was supported by the National Key R&D Program of China (2018YFB0904200), the National Natural Science Foundation of China (51577067), the Beijing Natural Science Foundation of China (3162033), the Hebei Natural Science Foundation of China (E2015502060), the State Key

Laboratory of Alternate Electrical Power System with Renewable Energy Sources (LAPS18008), the Headquarters Science and Technology Project of State Grid Corporation of China (SGCC)(NY7116021), the Open Fund of State Key Laboratory of Operation and Control of Renewable Energy & Storage Systems (China Electric Power Research Institute) (5242001600FB), the Fundamental Research Funds for the Central Universities (2018QN077). J.P.S. Catalão acknowledges the support by FEDER funds through COMPETE 2020 and by Portuguese funds through FCT, under Projects SAICT-PAC/0004/2015 - POCI-01-0145-FEDER-016434, POCI-01-0145-FEDER-006961, UID/EEA/50014/2013, UID/CEC/50021/2013, UID/EMS/00151/2013, and 02/SAICT/2017 - POCI-01-0145-FEDER-029803, and also funding from the EU 7th Framework Programme FP7/2007-2013 under GA no. 309048.

REFERENCES

[1] REN21, "Renewables 2016 Global Status Report," 2016.

[2] International Energy Agency, Renewables Information 2017. OECD Publishing, 2017.

[3] F. Wang, L. Zhou, H. Ren, and X. Liu, "Search Improvement Process-Chaotic Optimization-Particle Swarm Optimization-Elite Retention Strategy and Improved Combined Cooling-Heating-Power Strategy Based Two-Time Scale Multi-Objective Optimization Model for Stand-Alone Microgrid Operation," Energies, vol. 10, no. 12, p. 1936, Nov. 2017.

[4] F. Wang, Z. Zhen, B. Wang, and Z. Mi, "Comparative Study on KNN and SVM Based Weather Classification Models for Day Ahead Short Term Solar PV Power Forecasting," Appl. Sci., vol. 8, p. 28, Dec. 2017.

[5] L. Nonnenmacher, A. Kaur, and C. F. M. Coimbra, "Day-ahead resource forecasting for concentrated solar power integration," Renew. Energy, vol. 86, pp. 866–876, 2016.

[6] M. Rana, I. Koprinska, and V. G. Agelidis, "Univariate and multivariate methods for very short-term solar photovoltaic power forecasting," Energy Convers. Manag., vol. 121, pp. 380–390, 2016.

[7] Y. Sun, F. Wang, B. Wang, Q. Chen, N. A. Engerer, and Z. Mi, "Correlation Feature Selection and Mutual Information Theory Based Quantitative Research on Meteorological Impact Factors of Module Temperature for Solar Photovoltaic Systems," Energies, vol. 10, no. 1, p. 7, Dec. 2016.

[8] F. Wang, Z. Mi, S. Su, and H. Zhao, "Short-term solar irradiance forecasting model based on artificial neural network using statistical feature parameters," Energies, vol. 5, no. 5, pp. 1355–1370, 2012.

[9] F. Wang, H. Xu, T. Xu, K. Li, M. Shafie-khah, and J. P. S. Catalão, "The values of market-based demand response on improving power system reliability under extreme circumstances," Appl. Energy, vol. 193, pp. 220–231, 2017.

[10] Q. Chen et al., "Dynamic Price Vector Formation Model Based Automatic Demand Response Strategy for PV-assisted EV Charging Station," IEEE Trans. Smart Grid, pp. 1–1, 2017.

[11] F. Wang et al., "Multi-objective Optimization Model of Source-Load-Storage Synergetic Dispatch for Building Energy System Based on TOU Price Demand Response," IEEE Trans. Ind. Appl., vol. 54, no. 2, pp. 1017–1028, 2018.

[12] F. Wang, L. Zhou, B. Wang, Z. Wang, M. Shafie-khah, and J. Catalão, "Modified Chaos Particle Swarm Optimization-Based Optimized Operation Model for Stand-Alone CCHP Microgrid," Appl. Sci., vol. 7, no. 8, p. 754, 2017.

[13] F. Wang, Z. Zhen, Z. Mi, H. Sun, S. Su, and G. Yang, "Solar irradiance feature extraction and support vector machines based weather status pattern recognition model for short-term photovoltaic power forecasting," Energy Build., vol. 86, pp. 427–438, 2015.

[14] C. W. Chow et al., "Intra-hour forecasting with a total sky imager at the UC San Diego solar energy testbed," Sol. Energy, vol. 85, no. 11, pp. 2881–2893, 2011.

[15] M. Yabuki, M. Shiobara, K. Nishinaka, and M. Kuji, "Development of a cloud detection method from whole-sky color images," Polar Sci., vol. 8, no. 4, pp. 315–326, 2014.

[16] R. Marquez and C. F. M. Coimbra, "Intra-hour DNI forecasting based on cloud tracking image analysis," Sol. Energy, vol. 91, pp. 327–336, 2013.

[17] F. Wang et al., "Image phase shift invariance based cloud motion displacement vector calculation method for ultra-short-term solar PV power forecasting," Energy Convers. Manag., vol. 157, pp. 123–135, Feb. 2018.

[18] P. Tzoumanikas, E. Nikitidou, A. F. Bais, and A. Kazantzidis, "The effect of clouds on surface solar irradiance, based on data from an all-sky imaging system," Renew. Energy, vol. 95, pp. 314–322, Sep. 2016.

[19] A. T. Lorenzo, W. F. Holmgren, and A. D. Cronin, "Irradiance forecasts based on an irradiance monitoring network, cloud motion, and spatial averaging," Sol. Energy, vol. 122, pp. 1158–1169, 2015.

[20] S. Quesada-Ruiz, Y. Chu, J. Tovar-Pescador, H. T. C. Pedro, and C. F. M. Coimbra, "Cloud-tracking methodology for intra-hour DNI forecasting," Sol. Energy, vol. 102, pp. 267–275, 2014.

[21] G. C. Vliet, "Principles of Solar Engineering," Journal of Solar Energy Engineering, vol. 122, no. 2. p. 114, 2000.

[22] V. P. A. Lonij, A. E. Brooks, A. D. Cronin, M. Leuthold, and K. Koch, "Intra-hour forecasts of solar power production using measurements from a network of irradiance sensors," Sol. Energy, vol. 97, pp. 58–66, 2013.

[23] X. Feng, Q. Li, Y. Zhu, J. Hou, L. Jin, and J. Wang, "Artificial neural networks forecasting of PM2.5 pollution using air mass trajectory based geographic model and wavelet transformation," Atmos. Environ., vol. 107, pp. 118–128, 2015.

[24] Z. Men, E. Yee, F.-S. Lien, D. Wen, and Y. Chen, "Short-term wind speed and power forecasting using an ensemble of mixture density neural networks," Renew. Energy, vol. 87, pp. 203–211, 2016.

[25] S. Karsoliya, "Approximating Number of Hidden layer neurons in Multiple Hidden Layer BPNN Architecture," Int. J. Eng. Trends Technol., vol. 3, no. 6, pp. 714–717, 2012.

[26] B. Y. Qu, B. F. Lang, J. J. Liang, A. K. Qin, and O. D. Crisalle, "Two-Hidden-Layer Extreme Learning Machine for Regression and Classification," Neurocomputing, vol. 175, pp. 826–834, 2015.

[27] G. Bin Huang, "Learning capability and storage capacity of two-hidden-layer feedforward networks," IEEE Trans. Neural Networks, vol. 14, no. 2, pp. 274–281, 2003.

[28] M. G. De Giorgi, P. M. Congedo, M. Malvoni, and D. Laforgia, "Error analysis of hybrid photovoltaic power forecasting models: A case study of mediterranean climate," Energy Convers. Manag., vol. 100, pp. 117–130, 2015.